Solar Cells

DOI: 10.1002/anie.201409877

Application of the Tris(acetylacetonato)iron(III)/(II) Redox Couple in p-Type Dye-Sensitized Solar Cells**

Ishanie Rangeeka Perera, Torben Daeneke, Satoshi Makuta, Ze Yu, Yasuhiro Tachibana, Amaresh Mishra, Peter Bäuerle, C. André Ohlin, Udo Bach, and Leone Spiccia**

Abstract: *An electrolyte based on the tris(acetylacetonato)-iron(III)/(II) redox couple ($[Fe(acac)_3]^{0/1-}$) was developed for p-type dye-sensitized solar cells (DSSCs). Introduction of a NiO blocking layer on the working electrode and the use of chenodeoxycholic acid in the electrolyte enhanced device performance by improving the photocurrent. Devices containing $[Fe(acac)_3]^{0/1-}$ and a perylene–thiophene–triphenylamine sensitizer (PMI–6T–TPA) have the highest reported short-circuit current ($J_{SC} = 7.65\ mA\,cm^{-2}$), and energy conversion efficiency (2.51 %) for p-type DSSCs coupled with a fill factor of 0.51 and an open-circuit voltage $V_{OC} = 645\ mV$. Measurement of the kinetics of dye regeneration by the redox mediator revealed that the process is diffusion limited as the dye-regeneration rate constant ($1.7 \times 10^8\ M^{-1}\,s^{-1}$) is very close to the maximum theoretical rate constant of $3.3 \times 10^8\ M^{-1}\,s^{-1}$. Consequently, a very high dye-regeneration yield (> 99 %) could be calculated for these devices.*

The possibility of achieving high energy conversion efficiencies and low manufacturing costs continues to stimulate interest in dye-sensitized solar cells (DSSCs).[1] In p-type DSSCs, the photocathode consists of a nanostructured p-type semiconductor sensitized with a dye to efficiently capture solar energy. On photoexcitation, the sensitizer injects holes into the valence band of the p-type semiconductor (typically NiO).[2] In other words, electrons flow from the semiconductor valence band to the sensitizer. The oxidized redox mediator then oxidizes the reduced dye molecules back to their original state and injects electrons into the counter electrode. The electrons then flow through the external circuit and enter the device at the working electrode completing the cycle. Energy conversion efficiencies of up to 13 % have been reported for n-type DSSCs[3] whereas p-type DSSCs have reached 1.3 %.[2c] This difference is largely due to drawbacks associated with the electrolytes used to date and the NiO semiconductor. Being highly colored and electrochromic, NiO absorbs a substantial amount of visible light, decreasing the amount of light available for absorption by the sensitizer.[4]

Typically, electrolytes based on the I_3^-/I^- redox couple have been used as the redox mediator in p-type DSSCs. This limits the open-circuit voltage (V_{OC}) that can be achieved to approximately 300 mV because of the small energy gap (Figure 1c) between the redox potential of the I_3^-/I^- couple (+0.32 V vs. NHE; NHE = normal hydrogen electrode) and the valence band edge of NiO (+0.70 V vs. NHE).[5] For these devices a maximum efficiency of 0.61 % has been achieved.[6] Attempts were made to substitute the I_3^-/I^- redox mediator with cobalt polypyridyl complexes[7] and disulfide/thiolates,[8] however the device performance could not be improved until $[Co(en)_3]^{3+/2+}$ (en = 1,2-diaminoethane) was introduced. Devices based on this redox mediator (denoted $[Co(en)_3]$-p-DSSCs) and the PMI–6T–TPA sensitizer (Figure 1a) have recently reached efficiencies of 1.3 %.[2c] PMI–6T–TPA has been the best performing sensitizer for p-type DSSCs owing to its more long-lived charge-separated state when compared

[*] I. R. Perera, Dr. C. A. Ohlin, Prof. Dr. L. Spiccia
School of Chemistry, Monash University
Victoria 3800 (Australia)
E-mail: leone.spiccia@monash.edu
Dr. T. Daeneke, Prof. Dr. U. Bach
CSIRO Materials Science and Engineering
CSIRO Future Manufacturing Flagship, Bag 10
Clayton South 3169 Victoria (Australia)
Dr. Z. Yu, Prof. Dr. U. Bach
Department of Materials Engineering, Faculty of Engineering
Monash University, Victoria 3800 (Australia)
E-mail: udo.bach@monash.edu
Prof. Dr. U. Bach
Melbourne Centre for Nanofabrication
151 Wellington Road, Clayton 3168 Victoria (Australia)
S. Makuta, Prof. Dr. Y. Tachibana
School of Aerospace, Mechanical and Manufacturing Engineering
RMIT University, Bundoora, Victoria 3083 (Australia)
Prof. Dr. Y. Tachibana
Japan Science and Technology Agency (JST), PRESTO
4-1-8 Honcho Kawaguchi, Saitama 332-0012 (Japan)
Dr. A. Mishra, Prof. Dr. P. Bäuerle
Institute for Organic Chemistry II and Advanced Materials
University of Ulm, Albert-Einstein-Allee 11, 89081 Ulm (Germany)

[**] We acknowledge financial support from the Australian Solar Institute, Victorian State Government Department of Primary Industry, Bluescope Steel, Innovia Films, Innovia Security, and Bosch (Victorian Organic Solar Cells consortium), and Monash University (for providing I.R.P. with an International Postgraduate Research Scholarship and an Australian Postgraduate Award). Support of the Australian Centre for Advanced Photovoltaics by the Australian Government through the Australian Renewable Energy Agency (ARENA) is also gratefully acknowledged. C.A.O. thanks the Australian Research Council for Discovery project grants DP110105530 and DP130100483, and a QEII fellowship. The Monash center for electron microscopy is also acknowledged for the SEM facilities. We thank Iacopo Benesperi for calculations of the optimized geometries and molecular radii and Dr. Monika Fekete for the SEM analyses.

Supporting information for this article is available on the WWW under http://dx.doi.org/10.1002/anie.201409877.

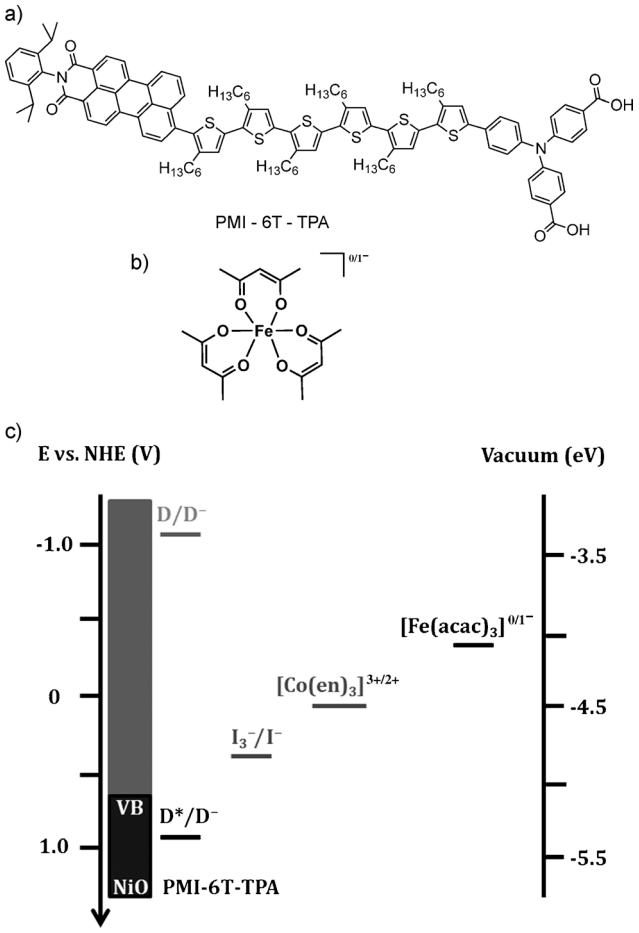

Figure 1. Molecular structures of a) PMI–6T–TPA and b) $[Fe(acac)_3]^{0/1-}$. c) The energy-level diagram of p-type DSSC components and approximate redox potentials of the electrolytes based on $[Fe(acac)_3]^{0/1-}$, $[Co(en)_3]^{3+/2+}$, and I_3^-/I^-. Redox potentials are reported relative to the NHE. VB = valence band. D = dye.

to other reported sensitizers.[9] This feature enhances device performance by decreasing interfacial charge-recombination reactions.[9,10] Indeed, the highest short-circuit current (J_{SC} = 7.0 mA cm^{-2}) for p-type DSSCs has been achieved using PMI–6T–TPA in conjunction with I_3^-/I^- and by replacing the NiO nanoparticles with NiO microballs.[2b]

Herein, we report efficient p-type DSSCs based on the readily available and inexpensive coordination complex tris(acetylacetonato)iron(III)/(II) ($[Fe(acac)_3]^{0/1-}$, Figure 1 b).[11] The $[Fe(acac)_3]^{0/1-}$ couple has a redox potential of −0.20 V versus NHE. This is closer to the LUMO (lowest unoccupied molecular orbital) level of the sensitizer while still providing sufficient energy (approximately 500 mV) for dye regeneration. In terms of the energetics, it should therefore be a more suitable mediator for p-type DSSCs than either $[Co(en)_3]^{3+/2+}$ (−0.03 V vs. NHE)[2c] or I_3^-/I^-. Additionally, the acetylacetonato ligand offers the opportunity to fine-tune the redox potential of the complex through simple substitution at various positions within its organic framework. The optimized $[Fe(acac)_3]^{0/1-}$-based devices constructed using the PMI–6T–TPA sensitizer have achieved an energy conversion efficiency of 2.51 ± 0.08 %.

Devices were initially constructed using a NiO photocathode working electrode (WE) sensitized with PMI–6T–TPA, a platinized counter electrode (CE), and an electrolyte composed of $(NBu_4)[Fe(acac)_3]$ (0.20 M), $[Fe(acac)_3]$ (0.10 M), 4-*tert*-butylpyridine (tBP; 0.50 M), and lithium bis(trifluoromethanesulfonyl)imide (LiTFSI; 0.10 M). These devices achieved efficiencies of 1.57 ± 0.23 % (see Table S1 in the Supporting Information).

A blocking layer is commonly employed in n-type DSSCs to decrease detrimental charge-recombination reactions occurring at the FTO–electrolyte interface (FTO = fluorine-doped tin oxide).[12] An increase in the device performance has also been reported by applying the same approach in p-type devices.[13] A new NiO blocking layer was developed in this work which utilized the spray pyrolysis of $[Ni(acac)_2]$ to deposit a thin layer of NiO (approximately 10 nm, determined from scanning electron microscopy) on the FTO glass prior to printing of the mesoporous NiO film (Figure S5). This treatment resulted in an increase in the average J_{SC} values from 5.68 ± 0.49 mA cm^{-2} to 6.95 ± 0.20 mA cm^{-2}, the fill factor (FF) from 0.43 ± 0.02 to 0.49 ± 0.02, and the overall efficiency from 1.57 ± 0.23 % to 2.03 ± 0.03 % (see Table S1) for devices applying the $[Fe(acac)_3]^{0/1-}$ redox mediator ($[Fe(acac)_3]$-p-DSSCs). An optimum thickness for the porous NiO layer of approximately 4.2 μm was determined by constructing devices with varying NiO thicknesses (see Table S2).

Chenodeoxycholic acid (**1**) has been used as an electrolyte additive in n-type DSSCs to decrease interfacial charge-recombination reactions through passivation of the TiO_2 surface.[14] Salvatori et al. concluded that molecules of **1** achieve this by forming supramolecular aggregates on the TiO_2 surface, thereby limiting the access of reduced species in the electrolyte.[15] In this study, the addition of **1** increased the J_{SC} value from 6.95 ± 0.20 mA cm^{-2} to 7.65 ± 0.39 mA cm^{-2} and the V_{OC} value from 595 ± 6 mV to 645 ± 12 mV (see Table S1 and Figure S6). This resulted in a substantial increase in device efficiency to 2.51 ± 0.08 %. Thus, **1** as an electrolyte additive clearly has a beneficial effect in NiO-based p-type DSSCs. Surface passivation of the NiO surface by **1** was confirmed by measuring the ATR–FTIR spectra (ATR = attenuated total reflection) of NiO films that had been dipped in a solution of **1** (10 mM), as is present in the optimized electrolyte. The spectra measured after various exposure times showed the appearance and increase of bands at around 1400 cm^{-1} and 1600 cm^{-1} (Figure S7). These correspond to symmetric and asymmetric stretches of the COO^- group, respectively. The band positions further indicate that the carboxylate groups on **1** coordinate to nickel centers on the NiO surface.[16] Additionally, stretching bands at approximately 2900 cm^{-1} can be attributed to CH_2/CH groups on the backbone of **1**.

The performance of the optimized $[Fe(acac)_3]$-p-DSSCs was compared with that of cells made with the I_3^-/I^- and $[Co(en)_3]^{3+/2+}$ redox shuttles (see Table 1 and Figure S8). For the devices based on the I_3^-/I^- couple, a high J_{SC} value was achieved but the efficiency was limited to 0.60 ± 0.02 % (under simulated 100 % sun conditions) by a low V_{OC} value and fill factor. For $[Co(en)_3]^{3+/2+}$, a higher V_{OC} value was achieved compared to the other two devices. The DSSCs with

Table 1: Photovoltaic parameters for p-type DSSCs prepared with electrolytes based on the I_3^-/I^-, $[Co(en)_3]^{3+/2+}$, and $[Fe(acac)_3]^{0/1-}$ redox couples and the PMI–6T–TPA dye measured under simulated 10% sun and 100% sun (1000 $W m^{-2}$) irradiation.

10% sun	I_3^-/I^-	$[Co(en)_3]^{3+/2+}$	$[Fe(acac)_3]^{0/1-}$
V_{oc} [mV]	179 ± 15	634 ± 6	519 ± 15
J_{sc} [mA cm^{-2}]	0.77 ± 0.03	0.55 ± 0.02	0.83 ± 0.03
FF	0.39 ± 0.04	0.44 ± 0.02	0.60 ± 0.01
Efficiency [%]	0.53 ± 0.10	1.52 ± 0.03	2.55 ± 0.06
100% sun	I_3^-/I^-	$[Co(en)_3]^{3+/2+}$	$[Fe(acac)_3]^{0/1-}$
V_{oc} [mV]	243 ± 10	724 ± 6	645 ± 12
J_{sc} [mA cm^{-2}]	6.26 ± 0.14	4.11 ± 0.35	7.65 ± 0.39
FF	0.39 ± 0.01	0.40 ± 0.01	0.51 ± 0.01
Efficiency [%]	0.60 ± 0.02	1.20 ± 0.03	2.51 ± 0.08

Photocathode NiO film thickness = 4.2 μm. Thermally decomposed Pt on FTO glass was used as the counter electrode. *I–V* data were measured with settling times of 1 s for I_3^-/I^-, 4 s for $[Co(en)_3]^{3+/2+}$ and 2 s for $[Fe(acac)_3]^{0/1-}$ devices. The I_3^-/I^- electrolyte contained I_2 (0.03 M), tBP (0.50 M), 1-butyl-3-methylimidazolium iodide (0.60 M), and guanidium thiocyanate (0.10 M) in acetonitrile. The $[Co(en)_3]^{3+/2+}$ electrolyte contained $[Co(en)_3](BF_4)_2$ (0.30 M; prepared in situ using $Co(BF_4)_2{\cdot}6H_2O$ (0.30 M) and 1,2-diaminoethane (1.67 M)), $[Co(en)_3](BF_4)_3$ (0.07 M), and LiTFSI (0.10 M) in acetonitrile. The $[Fe(acac)_3]^{0/1-}$ electrolyte contained $(NBu_4)[Fe(acac)_3]$ (0.10 M), $[Fe(acac)_3]$ (0.05 M), tBP (0.25 M), LiTFSI (0.05 M), and chenodeoxycholic acid (0.010 M) in acetonitrile. Average photovoltaic parameters are listed with standard errors derived from ≥3 different cells.

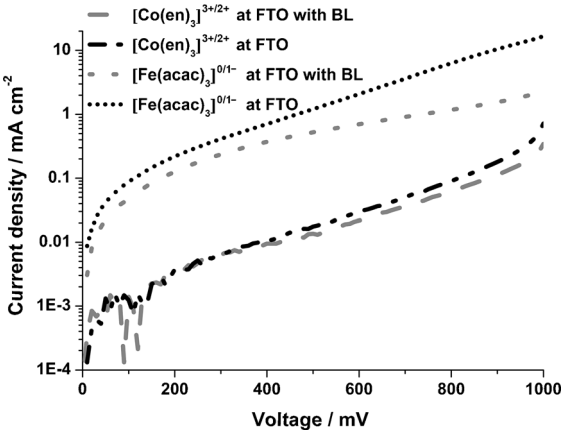

Figure 2. Dependence of the current density of the devices based on the $[Fe(acac)_3]^{0/1-}$ and $[Co(en)_3]^{3+/2+}$ electrolytes on different applied bias under dark conditions. BL = blocking layer.

$[Co(en)_3]^{3+/2+}$ performed better under low light conditions (10% sun), achieving an efficiency of 1.52 ± 0.03%, compared to 1.20 ± 0.03% at 100% sun illumination (simulated sunlight AM 1.5 G, 1000 $W m^{-2}$). In comparison, the 2.51 ± 0.08% efficiency achieved for $[Fe(acac)_3]$-p-DSSCs is almost double the best reported to date.[2c]

Based on the redox potentials of the electrolytes, the highest V_{OC} value would be expected for devices constructed with $[Fe(acac)_3]^{0/1-}$ ($E_{red/ox} = -0.20$ V vs. NHE). In contrast, the data obtained from current–voltage plots (*I–V* plots) show that the V_{OC} value for $[Fe(acac)_3]$-p-DSSCs is lower than for $[Co(en)_3]$-p-DSSCs ($E_{red/ox} = -0.03$ V vs. NHE). This discrepancy appears to suggest that the V_{OC} of $[Fe(acac)_3]$-p-DSSCs is affected by recombination phenomena across either the NiO/electrolyte or the FTO/electrolyte interface. To test the hypothesis that charge recombination across the exposed areas of the FTO back contact contributes to the measured effects, the dark currents across FTO/electrolyte junctions for $[Fe(acac)_3]^{0/1-}$ and $[Co(en)_3]^{3+/2+}$ electrolytes were compared in the presence and absence of a dense NiO layer. Dark currents were recorded in two-terminal sandwich cells with a platinized counter electrode. The data shown in Figure 2 reveal that the leakage currents across the bare FTO/electrolyte interface in $[Fe(acac)_3]$-p-DSSCs are about two orders of magnitude higher than those detected for $[Co(en)_3]$-p-DSSCs across the measured voltage bias range. This clearly indicates that charge recombination across this junction plays a significant role in $[Fe(acac)_3]$-p-DSSCs. At a voltage bias of 645 mV, equivalent to the open-circuit voltage of $[Fe(acac)_3]$-p-DSSCs, current densities as high as 2.74 mA cm^{-2} and 0.80 mA cm^{-2} can be measured in the absence and the presence of the dense NiO layer, respectively. Therefore, charge recombination across the FTO–electrolyte interface limits the open-circuit voltages observed in $[Fe(acac)_3]$-p-DSSCs. The higher charge recombination can be explained by the attraction of the negatively charged $[Fe(acac)_3]^{1-}$ complex to holes injected into the NiO layer. This reduced species has a higher affinity for the holes than the positively charged $[Co(en)_3]^{2+}$ complex. Moreover, electron-transfer processes associated with the $[Co(en)_3]^{3+/2+}$ redox couple involves a higher energy barrier because of a high-to-low spin transition. In contrast, there is no such transition for the $[Fe(acac)_3]^{0/1-}$ couple as both complexes exist in the high-spin state. In keeping with this, the deposition of a dense NiO layer significantly decreases charge recombination across the FTO back-contact electrode for the $[Fe(acac)_3]$-p-DSSCs. On the other hand, the introduction of a dense NiO layer in $[Co(en)_3]$-p-DSSCs has only a very minor influence on the leakage currents across the FTO back contact. Optimization of the NiO blocking layer should lead to a further decrease in charge recombination in $[Fe(acac)_3]$-p-DSSCs and accordingly to an increase in V_{OC} and FF values and cell efficiencies.

The incident photon-to-current conversion efficiency (IPCE) is a measure of the number of electrons collected under short-circuit conditions per number of incident photons at a given wavelength of the incident monochromatic light (equivalent to <2% sun). The IPCE data in Figure 3 correlate well with the J_{SC} values measured at 10% sun. The $[Fe(acac)_3]$-p-DSSCs show a higher IPCE (57%) than those based on $[Co(en)_3]^{3+/2+}$ and I_3^-/I^-. As expected from the measured photocurrents, the $[Co(en)_3]$-p-DSSCs showed the lowest IPCE (44%).

Transient absorption spectroscopy was carried out on devices based on the $[Fe(acac)_3]^{0/1-}$ redox couple to further understand the charge-recombination kinetics and to rationalize the origin of the superior performance of these devices. Studies in the absence of the redox couple were used to determine the recombination rate of the photoreduced dye anion with holes in the NiO valence band. An observed rate constant (k_{obs}) of $1.04 \pm 0.10 \times 10^4$ s^{-1} was determined under short-circuit conditions (Figure S9 and Table S3). Studies

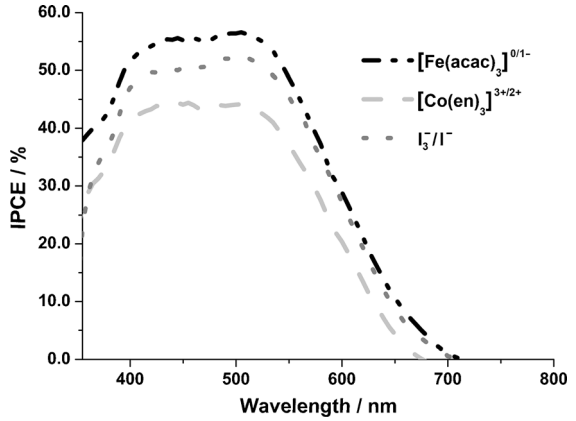

Figure 3. IPCE measurements under low light conditions (<2% sun) of DSSCs based on I_3^-/I^-, $[Co(en)_3]^{3+/2+}$, and $[Fe(acac)_3]^{0/1-}$ electrolytes sensitized with the dye PMI–6T–TPA.

were then carried out in the presence of the $[Fe(acac)_3]^{0/1-}$ redox shuttle to estimate the dye regeneration rate (k_{reg}). A k_{reg} value of $1.70 \pm 0.28 \times 10^8\,M^{-1}s^{-1}$ was calculated under short-circuit conditions which is over 50 times higher than the value of $3.0 \times 10^6\,M^{-1}s^{-1}$ reported for $[Co(en)_3]$-p-DSSCs.[18] A faster dye-regeneration rate can lead to a decrease in recombination between the photoreduced dye anion and holes in the NiO valence band, leading to a higher J_{SC} value for devices based on $[Fe(acac)_3]^{0/1-}$.

A study of the dependence of the regeneration rate on $[Fe(acac)_3]$ concentration was carried out under short-circuit conditions (Figure 4, Figure S10, and Tables S4 and S5) to further understand the dye-regeneration kinetics. Similar k_{reg} values were obtained for devices with $[Fe(acac)_3]$ concentrations varying from 1 mM to 50.0 mM. This confirmed that dye regeneration shows a classical first-order dependence on $[Fe(acac)_3]$ concentration. To estimate the theoretical diffusion-limited rate constant (k_D) for $[Fe(acac)_3]$ in acetonitrile, the Randles–Servick equation[17] was used to determine diffusion coefficient for $[Fe(acac)_3]$. An average value of $(7.10 \pm 0.78) \times 10^{-6}\,cm^2s^{-1}$ was calculated in acetonitrile from

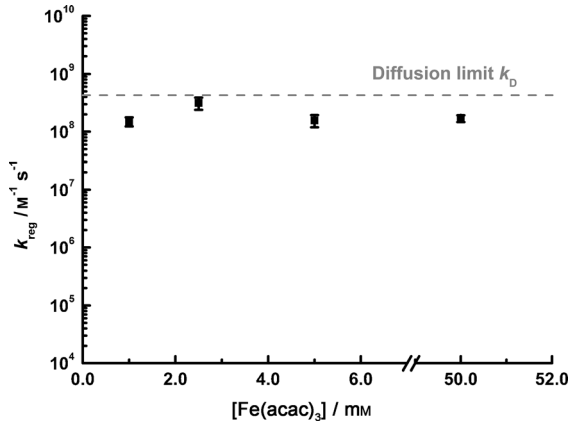

Figure 4. Dependence of the bimolecular dye-regeneration rate constant k_{reg} on the concentration of $[Fe(acac)_3]$ in the electrolyte with no applied bias.

the scan-rate dependence of the peak currents (see Table S6). Applying this value and using estimated radii for $[Fe(acac)_3]$ and PMI–6T–TPA of 4.5 Å and 9.5 Å, respectively, a maximum theoretical rate constant, k_D, of $3.3 \times 10^8\,M^{-1}s^{-1}$, was calculated. The good agreement of the experimental k_{reg} value with this value suggests that dye regeneration is mostly limited by diffusion. For $[Co(en)_3]^{3+}$ in acetonitrile, however, the calculated diffusion coefficient was lower $(8.26 \pm 0.60) \times 10^{-7}\,cm^2s^{-1}$ (Table S7). The higher diffusion coefficient (approximately 10-fold) and much higher (>50 times) dye-regeneration rate for $[Fe(acac)_3]$ explain the enhanced current density measured in the $[Fe(acac)_3]$-p-DSSCs compared to $[Co(en)_3]$-p-DSSCs. Finally, the k_{reg} values were used to estimate the dye-regeneration yield (Φ) for the $[Fe(acac)_3]^{0/1-}$ devices. The original device (50.0 mM of $[Fe(acac)_3]$) showed $\Phi = 99.9\%$, further highlighting the ability of the iron(III) complex to rapidly regenerate the dye within these devices.

In conclusion, we have applied $[Fe(acac)_3]^{0/1-}$ as redox mediator in p-type DSSCs in conjunction with the PMI–6T–TPA sensitizer. Solar cells incorporating a NiO blocking layer and chenodeoxycholic acid as an electrolyte additive yielded energy conversion efficiencies of $2.51 \pm 0.08\%$. To our knowledge, this is the highest reported efficiency for a p-type DSSC. Open-circuit voltages of $[Fe(acac)_3]$-p-DSSCs were lower than those measured for $[Co(en)_3]$-p-DSSCs, despite a 170 mV more negative redox potential of $[Fe(acac)_3]^{0/1-}$ compared to $[Co(en)_3]^{3+/2+}$. The up to two orders of magnitude faster charge recombination across the FTO/electrolyte, even in presence of a NiO blocking layer, was identified as one factor responsible for the relatively low photovoltage detected in $[Fe(acac)_3]$-p-DSSCs. Transient absorption spectroscopy studies further revealed that the rate of dye regeneration by the $[Fe(acac)_3]$ complex is diffusion limited, quantitative (>99%), and about 50 times faster than measured for $[Co(en)_3]^{3+}$. The development of efficient p-type devices is important as it could pave the way to the construction of tandem p–n-DSSCs combining dye-sensitized photoanodes and photocathodes. These have theoretical performance limits well beyond that of simple single-junction DSSCs. The low efficiency of p-type DSSCs currently represents a major impediment towards the realization of efficient tandem DSSCs. Further work is required to further bridge the efficiency gap between p-type DSSCs and n-type DSSCs and to make tandem DSSCs a viable alternative to single-junction DSSCs.

Experimental Section

The photocathodes were prepared by sensitizing the screen printed NiO film with PMI–6T–TPA. The devices were constructed by sealing a sensitized NiO photocathode and a platinized anode with a 25 μm thick 6×6 mm Surlyn gasket (Solaronix). The electrolyte was inserted into the device by vacuum backfilling. Compositions of the I_3^-/I^-, $[Co(en)_3]^{3+/2+}$, and $[Fe(acac)_3]^{0/1-}$ electrolytes are given in the footnote of Table 1. Exclusion of oxygen was important in the preparation of the electrolytes based on the $[Fe(acac)_3]^{0/1-}$ and $[Co(en)_3]^{3+/2+}$ redox couples and in device construction. The *I–V* data was measured with a settling time of 1 s for I_3^-/I^-, 4 s for $[Co(en)_3]^{3+/2+}$, and 2 s for $[Fe(acac)_3]^{0/1-}$ devices. Transient absorption spectroscopy was per-

formed on devices constructed with electrolytes containing varying concentrations of [Fe(acac)$_3$] (50.0 mM, 5.0 mM, 2.5 mM).

Received: October 8, 2014
Revised: November 29, 2014
Published online: January 29, 2015

Keywords: dye-sensitized solar cells · energy conversion · iron · redox chemistry · semiconductors

[1] M. Grätzel, *Nature* **2001**, *414*, 338 – 344.
[2] a) A. Nattestad, M. Ferguson, R. Kerr, Y.-B. Cheng, U. Bach, *Nanotechnology* **2008**, *19*, 295304; b) S. Powar, Q. Wu, M. Weidelener, A. Nattestad, Z. Hu, A. Mishra, P. Bauerle, L. Spiccia, Y.-B. Cheng, U. Bach, *Energy Environ. Sci.* **2012**, *5*, 8896 – 8900; c) S. Powar, T. Daeneke, M. T. Ma, D. Fu, N. W. Duffy, G. Götz, M. Weidelener, A. Mishra, P. Bäuerle, L. Spiccia, U. Bach, *Angew. Chem. Int. Ed.* **2013**, *52*, 602 – 605; *Angew. Chem.* **2013**, *125*, 630 – 633.
[3] S. Mathew, A. Yella, P. Gao, R. Humphry-Baker, B. F. Curchod, N. Ashari-Astani, I. Tavernelli, U. Rothlisberger, M. K. Nazeeruddin, M. Grätzel, *Nat. Chem.* **2014**, *6*, 242 – 247.
[4] a) J. Bai, X. Xu, L. Xu, J. Cui, D. Huang, W. Chen, Y. Cheng, Y. Shen, M. Wang, *ChemSusChem* **2013**, *6*, 622 – 629; b) L. Li, E. A. Gibson, P. Qin, G. Boschloo, M. Gorlov, A. Hagfeldt, L. Sun, *Adv. Mater.* **2010**, *22*, 1759 – 1762; c) M. Yu, G. Natu, Z. Ji, Y. Wu, *J. Phys. Chem. Lett.* **2012**, *3*, 1074 – 1078.
[5] a) H. Zhu, A. Hagfeldt, G. Boschloo, *J. Phys. Chem. C* **2007**, *111*, 17455 – 17458; b) Z. Xu, D. Xiong, H. Wang, W. Zhang, X. Zeng, L. Ming, W. Chen, X. Xu, J. Cui, M. Wang, S. Powar, U. Bach, Y.-B. Cheng, *J. Mater. Chem. A* **2014**, *2*, 2968 – 2976.
[6] X. L. Zhang, Z. Zhang, D. Chen, P. Bauerle, U. Bach, Y.-B. Cheng, *Chem. Commun.* **2012**, *48*, 9885 – 9887.
[7] E. A. Gibson, A. L. Smeigh, L. c. Le Pleux, L. Hammarström, F. Odobel, G. Boschloo, A. Hagfeldt, *J. Phys. Chem. C* **2011**, *115*, 9772 – 9779.
[8] X. Xu, B. Zhang, J. Cui, D. Xiong, Y. Shen, W. Chen, L. Sun, Y. Cheng, M. Wang, *Nanoscale* **2013**, *5*, 7963 – 7969.
[9] A. Nattestad, A. J. Mozer, M. K. R. Fischer, Y. B. Cheng, A. Mishra, P. Bäuerle, U. Bach, *Nat. Mater.* **2010**, *9*, 31 – 35.
[10] a) P. Qin, H. Zhu, T. Edvinsson, G. Boschloo, A. Hagfeldt, L. Sun, *J. Am. Chem. Soc.* **2008**, *130*, 8570 – 8571; b) P. Qin, J. Wiberg, E. A. Gibson, M. Linder, L. Li, T. Brinck, A. Hagfeldt, B. Albinsson, L. Sun, *J. Phys. Chem. C* **2010**, *114*, 4738 – 4748; c) E. A. Gibson, A. L. Smeigh, L. Le Pleux, J. Fortage, G. Boschloo, E. Blart, Y. Pellegrin, F. Odobel, A. Hagfeldt, L. Hammarström, *Angew. Chem. Int. Ed.* **2009**, *48*, 4402 – 4405; *Angew. Chem.* **2009**, *121*, 4466 – 4469; d) L. Le Pleux, A. L. Smeigh, E. Gibson, Y. Pellegrin, E. Blart, G. Boschloo, A. Hagfeldt, L. Hammarstrom, F. Odobel, *Energy Environ. Sci.* **2011**, *4*, 2075 – 2084.
[11] S. F. Chin, S. C. Pang, C. H. Tan, *J. Mater. Environ. Sci.* **2011**, *2*, 299 – 302.
[12] a) Y.-M. Sung, *Energy Procedia* **2013**, *34*, 582 – 588; b) E. Palomares, J. N. Clifford, S. A. Haque, T. Lutz, J. R. Durrant, *J. Am. Chem. Soc.* **2003**, *125*, 475 – 482.
[13] X. L. Zhang, F. Huang, A. Nattestad, K. Wang, D. Fu, A. Mishra, P. Bauerle, U. Bach, Y.-B. Cheng, *Chem. Commun.* **2011**, *47*, 4808 – 4810.
[14] a) T. Daeneke, T. H. Kwon, A. B. Holmes, N. W. Duffy, U. Bach, L. Spiccia, *Nat. Chem.* **2011**, *3*, 211 – 215; b) I. R. Perera, A. Gupta, W. Xiang, T. Daeneke, U. Bach, R. A. Evans, C. A. Ohlin, L. Spiccia, *Phys. Chem. Chem. Phys.* **2014**, *16*, 12021 – 12028.
[15] P. Salvatori, G. Marotta, A. Cinti, C. Anselmi, E. Mosconi, F. De Angelis, *J. Phys. Chem. C* **2013**, *117*, 3874 – 3887.
[16] G. B. Deacon, R. J. Phillips, *Coord. Chem. Rev.* **1980**, *33*, 227 – 250.
[17] T. Daeneke, A. J. Mozer, Y. Uemura, S. Makuta, M. Fekete, Y. Tachibana, N. Koumura, U. Bach, L. Spiccia, *J. Am. Chem. Soc.* **2012**, *134*, 16925 – 16928.
[18] T. Daeneke, Z. Yu, G. P. Lee, D. Fu, N. W. Duffy, S. Makuta, Y. Tachibana, L. Spiccia, A. Mishra, P. Bäuerle, U. Bach, *Adv. Energy Mater.* **2014**, DOI: 10.1002/aenm.201401387.

